

ACNet: Approaching-and-Centralizing Network for Zero-Shot Sketch-Based Image Retrieval

Hao Ren*
Fudan University
Shanghai, China
hren17@fudan.edu.cn

Ziqiang Zheng*
HKUST
Hong Kong, China
zhengziqiang1@gmail.com

Yang Wu
ARC Lab, Tencent PCG
Shenzhen, China
dylanywu@tencent.com

Hong Lu
Fudan University
Shanghai, China
honglu@fudan.edu.cn

Yang Yang
UESTC
Chengdu, China
dlyyang@gmail.com

Sai-Kit Yeung
HKUST
Hong Kong, China
saikit@ust.hk

Abstract

The huge domain gap between sketches and photos and the highly abstract sketch representations pose challenges for sketch-based image retrieval (SBIR). The zero-shot sketch-based image retrieval (ZS-SBIR) is more generic and practical but poses an even greater challenge because of the additional knowledge gap between the seen and unseen categories. To simultaneously mitigate both gaps, we propose an Approaching-and-Centralizing Network (termed “ACNet”) to jointly optimize sketch-to-photo synthesis and the image retrieval. The retrieval module guides the synthesis module to generate large amounts of diverse photo-like images which gradually approach the photo domain, and thus better serve the retrieval module than ever to learn domain-agnostic representations and category-agnostic common knowledge for generalizing to unseen categories. These diverse images generated with retrieval guidance can effectively alleviate the overfitting problem troubling concrete category-specific training samples with high gradients. We also discover the use of proxy-based NormSoftmax loss is effective in the zero-shot setting because its centralizing effect can stabilize our joint training and promote the generalization ability to unseen categories. Our approach is simple yet effective, which achieves state-of-the-art performance on two widely used ZS-SBIR datasets and surpasses previous methods by a large margin.

1. Introduction

Sketch-based image retrieval (SBIR) [2, 11, 21, 26, 43, 44] aims to perform cross-domain image retrieval among the

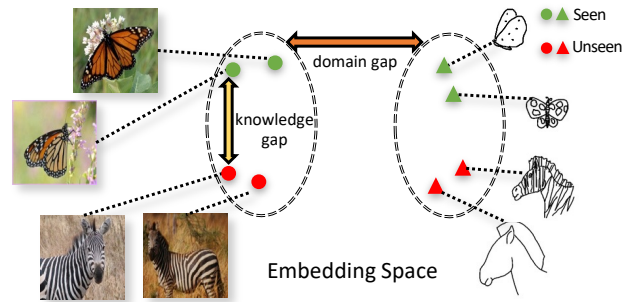


Figure 1. Two challenges in ZS-SBIR: 1) huge domain gap between sketches and photos; and 2) knowledge gap between seen categories and unseen categories.

photos and sketches drawn by humans. Touch-screen devices (e.g., smartphones and iPad) enable us to draw free-hand sketches conveniently. The drawn sketches are regarded as queries and the retrieval system can resort to returning some relevant photos according to the user’s intent. Considering the lack of colors, textures and detailed structural information, the sketches are highly *iconic*, *succinct* and *abstract*. The huge domain gap and the asymmetrical information between sketches and photos pose great challenges for SBIR. Since category labels provide a shortcut [24] for the retrieval model, the retrieval system may overfit the category label hence the retrieval problem would then turn into a classification problem. The follow-up zero-shot sketch-based image retrieval (ZS-SBIR) is introduced in [50] under a more practical and realistic setting, where the test data are from unseen categories. The knowledge gap between seen categories and unseen categories makes ZS-SBIR more intractable, as shown in Figure 1. The domain gap and knowledge gap are the two biggest challenges

*Both authors contributed equally to this research.

for ZS-SBIR.

To simultaneously mitigate the huge domain gap and knowledge gap, we design a novel, simple and effective **approaching and centralizing** network, which jointly trains sketch-to-photo synthesis and retrieval, as shown in Figure 2. The sketch-to-photo synthesis module encourages the retrieval module to focus more on domain-agnostic information for proper similarity measurement. This is done by constantly refining and feeding the synthesized photo-like images into the retrieval module during the training phase. Even though there are some noise and uncertainty introduced along with the synthesis, the continuously generated and refined images are of high diversity, which gradually **approach** the photo domain and thus benefit training a robust retrieval module that can overcome the domain gap.

The large amounts of synthesised images with high diversity can also force the retrieval module to better learn the common knowledge amongst the seen and unseen categories. It prevents the retrieval module from extracting the category-specific information and overfitting/remembering the specific details of the concrete training samples, which is catastrophic under the zero-shot setting. Therefore, our framework can also mitigate the knowledge gap and make the trained model generalize better.

Furthermore, we utilize the NormSoftmax [51] loss which has a class **centralization** effect to stabilize our joint training and promote the generalization capability to unseen categories. Previous pairwise losses (*e.g.*, Contrastive [18] and Triplet [14]) aim to optimize the model by sampling the informative pairs or triplets in one batch. It is easy for these methods to overfit the category-specific feature representations when the sampled training pairs or triplets have high gradients. The NormSoftmax assigns one proxy as the center point for each category and optimizes the model with the gradients from all the samples belonging to the assigned proxy. This loss function can better coordinate the relationship between all the samples from each category. Additionally, the noise and uncertainty introduced with the synthesis may cause difficulty in optimizing the pairwise losses. In contrast, the adopted NormSoftmax loss can better alleviate the influence of noise and uncertainty by proxy-based optimization [31, 39]. The proposed approaching (via sketch-to-photo synthesis) and centralizing (with the NormSoftmax loss) are mutually-beneficial, achieving a new state-of-the-art retrieval performance on two widely used ZS-SBIR datasets. To facilitate the development of ZS-SBIR, our codes will be released with the publication of this paper. Extensive ablation studies have been conducted to dissect our method.

Our main contributions can be summarized as follows:

- We propose an “Approaching-and-Centralizing Network (ACNet)” to integrate sketch-to-photo synthesis and retrieval through a joint training manner, in which

the synthesis module can better serve the downstream retrieval module than ever, and the retrieval module is able to guide the synthesis module to generate refined images gradually approaching the photo domain (mitigating the domain gap).

- We adopt the NormSoftmax loss to stabilize our joint training and promote the generalization ability under the zero-shot setting, thanks to its centralizing effect driven by proxy-based optimization.
- Comprehensive ZS-SBIR experiments and ablation studies on Sketchy Extended [50] and TU-Berlin Extended [37] datasets demonstrating the superiority of the proposed ACNet.

2. Related Work

2.1. SBIR

SBIR [11] has been studied for decades due to its commercial and realistic applications [3]. Attempts for solving the SBIR task mostly focus on bridging the domain gap between the sketches and photos, which can roughly be grouped in hand-crafted [11, 21] and cross-domain deep learning-based methods [13, 14, 18, 20, 41, 47]. Hand-crafted methods [11, 21] mostly work by extracting the edge map from natural photo images and then matching them with sketches using a Bag-of-Words model. Due to the large success and the robust recognition performance of deep learning methods, various specifically designed neural networks [2, 26, 30, 35, 43, 44] have been proposed for SBIR. The classical ranking losses, like contrastive loss [18, 47], triplet loss [14, 20] or classification loss [51] have also been introduced.

2.2. ZS-SBIR

SBIR requires all test categories to be seen during training, which cannot be guaranteed in real-world applications. The more challenging, generic and practical ZS-SBIR [37] task has attracted the attention of the computer vision community due to its real-world applications, in which the test categories do not appear in the training stage. Recent research [5, 8, 9, 42, 46, 50, 53] are exploring solutions for projecting the sketches and photos into a shared semantic space to perform accurate cross-domain image retrieval. However, the huge domain gap and the highly abstract sketch representations make it very difficult to perform ideal feature-level content-style disentanglement [5, 8, 9, 24] or bi-direction synthesis [29]. To bridge the knowledge gap between seen and unseen categories, existing methods [5, 7, 28, 49, 53, 55] introduced the semantic embeddings from the extra annotations to generate class prototypes for presenting the relationships between semantic categories in the common space. However, there is no explicit connection

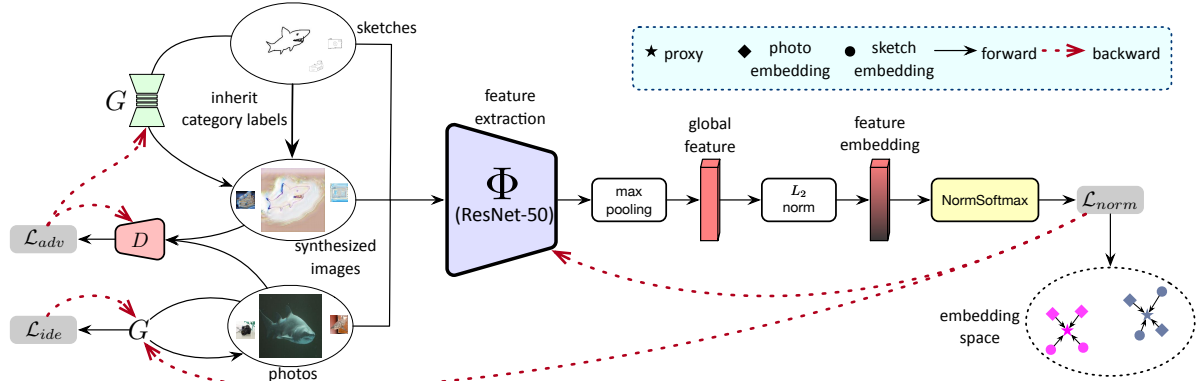


Figure 2. Overview of the proposed ACNet. The sketch-to-photo generator G aims to translate the sketches to the photo-like images while D is to distinguish whether the generated images are real photos and compute \mathcal{L}_{adv} . The identity loss \mathcal{L}_{ide} helps generate more photo-like images by forcing G to reconstruct the real photos. The main pipeline serves as the standard process for embedding learning. The embedding from the sketches, synthesized images and photos of the same class are enforced to be close to the assigned proxy, and far away from other proxies under the constraint of \mathcal{L}_{norm} . Different colors indicate the different classes. We design a joint training manner to integrate G and Φ . We refer the readers to check the forward and backward procedures to better understand our joint training scheme.

between the feature representations extracted from visual images and the semantic embeddings borrowed from the extra annotations. Furthermore, the semantic embeddings from the language models [16, 33] are computed based on word co-occurrence frequency. Sometimes these embeddings are not reliable [46] and cannot express the intra-class visual variation. In contrast to previous methods, we introduce the one-directional sketch-to-photo synthesis to mitigate the domain gap and promote the generalization ability in a joint training manner.

2.3. Sketch-to-photo Synthesis

Sketch-to-photo synthesis [4, 12, 27, 29, 45, 56] is a notably challenging task in the field of computer vision, which aims to generate photo-realistic images from the given abstract and exaggerated sketches. Sketch2Photo [3] proposed to compose new photo images through fusing the retrieved photo images from the given sketch. The semantic segmentation [1] and image blending [17] techniques were introduced to achieve the photo editing according to the user’s goal. The first deep learning-based free-hand sketch-to-photo synthesis is SketchyGAN [4], which aims to optimize an encoder-decoder model based on the aligned sketch-photo pairs. Ghosh *et al.* [15] proposed a multi-class photo generation based on incomplete edges or sketches. This method adopted a two-stage strategy for shape completion and appearance synthesis, which highly relies on paired training data. Sketchformer [34] designed a sequential sketch-to-photo generation model to promote the naturalness of the photo images. Liu *et al.* [29] conducted unsupervised sketch-to-photo synthesis and further analyzed the potential of adopting the synthesized images for retrieval. Ideally, a perfect sketch-to-photo generator could synthesize

the desired photo images with distinguishable and reliable feature representations for more accurate image retrieval, whilst preserving the intra-class and inter-class distribution after translation. However, the unsupervised domain translation performance is plagued by the huge domain gap as well as the highly abstract sketch representations. The translated photo images still suffer from visual artifacts [25] and noise even utilizing the semantic priors [25, 26, 52] and laborious generative networks [25, 34, 54]. Since the two modules are optimized separately, the noise and uncertainty introduced in the synthesis module could be propagated to the retrieval module and the error accumulation could heavily restrict the retrieval performance. Even if the generated images look realistic to humans, their benefits may not be able to surpass harms to the downstream retrieval task. Differently, our proposed ACNet jointly optimizes synthesis and retrieval, and thus ensures a significant performance boost.

3. Method

3.1. Problem Formulation

Consider n photos and m sketches denoted as $\mathcal{P} = \{(p_i, y_{p_i}) | y_{p_i} \in \mathcal{Y}\}_{i=1}^n$, and $\mathcal{S} = \{(s_i, y_{s_i}) | y_{s_i} \in \mathcal{Y}\}_{i=1}^m$ respectively. Under the SBIR setting, \mathcal{S} and \mathcal{P} are divided into the training set and test set with same category label set \mathcal{Y} . SBIR is to retrieve the best matched $p_j \in \mathcal{P}$ based on a query sketch s_i in \mathcal{S} , such that $y_{s_i} = y_{p_j}$. Under the ZS-SBIR setting, \mathcal{Y} is split into \mathcal{Y}_{tra} and \mathcal{Y}_{test} , in which there is no category overlap between \mathcal{Y}_{tra} and \mathcal{Y}_{test} ($\mathcal{Y}_{tra} \cap \mathcal{Y}_{test} = \emptyset$). The training data are $\mathcal{S}_{tra} = \{(s_i, y_{s_i}) | y_{s_i} \in \mathcal{Y}_{tra}\}$, $\mathcal{P}_{tra} = \{(p_i, y_{p_i}) | y_{p_i} \in \mathcal{Y}_{tra}\}$, and the test data are $\mathcal{S}_{test} = \{(s_i, y_{s_i}) | y_{s_i} \in \mathcal{Y}_{test}\}$,

$\mathcal{P}_{test} = \{(p_i, y_{p_i}) | y_{p_i} \in \mathcal{Y}_{test}\}$. The ZS-SBIR model is trained on data $(\mathcal{S}_{tra}, \mathcal{P}_{tra})$, and tested on $(\mathcal{S}_{test}, \mathcal{P}_{test})$.

3.2. Main Pipeline

We refer the readers to check the overall architecture of the proposed method in Figure 2.

Approaching by Sketch-to-photo Synthesis. Suppose the sketch s_i from \mathcal{S}_{tra} and the photo p_j from \mathcal{P}_{tra} , we first aim to generate a photo-like image $s_i^* = G(s_i)$ based on s_i through a generator $G : \mathcal{S}_{tra} \rightarrow \mathcal{P}_{tra}$. The adversarial loss of the GAN architecture can be expressed as:

$$\mathcal{L}_{adv}(G, D) = \mathbb{E}_{s_i, p_j \sim P_{data}(\mathcal{S}_{tra}, \mathcal{P}_{tra})} [\log D(p_j)] + \mathbb{E}_{s_i \sim P_{data}(\mathcal{S}_{tra})} [\log(1 - D(G(s_i)))] \quad (1)$$

where D is the discriminator to distinguish whether the image is from the real photo domain. The goal is to learn a mapping function, which could generate photo-like images that match the real photo distribution $P_{data}(\mathcal{P}_{tra})$. After the sketch-to-photo synthesis, we assign the category label of s_i to s_i^* . It is non-trivial to define such label-preserving synthesis-based transformations, especially when the uncertainty and noise have been introduced with the image synthesis. The synthesized images possess more texture and RGB information and thus gradually approach the photo domain, which can better serve cross-domain image retrieval. Considering there is no pixel-level constraint for G , G would tend to generate images with visual artifacts. To alleviate this problem, we design an identity loss \mathcal{L}_{ide} between p_j and $G(p_j)$, which is expressed as:

$$\mathcal{L}_{ide} = \mathbb{E}_{\mathcal{P}_{tra}} \|G(p_j) - p_j\|_1 \quad (2)$$

Since s_i and p_j share similar semantic contents (*e.g.*, the category and structure information), we can boost the synthesis performance by reconstructing the photos at the same time. With the full supervision from \mathcal{L}_{ide} , we could generate more photo-like images.

Feature Extraction. The sketch, generated image and real photo are fed into the backbone network to extract feature representations. Like previous methods, we adopt ResNet-50 [19] (denoted as Φ) as backbone. The outputs after max pooling are transformed into the desirable embedding dimension through a fully connected layer. L_2 -norm is adopted to obtain the final embedding for the retrieval task.

Centralizing with NormSoftmax. The NormSoftmax loss [51] is used as our objective function to increase the inter-class distance and reduce the intra-class distance over the photo and sketch set. Each category is assigned a learnable proxy. The final embedding x is enforced to be close to the proxy of its category, and far away from other proxies, as shown in Figure 2. The objective function is:

$$\mathcal{L}_{norm}(x) = -\log\left(\frac{\exp(\frac{x^T p_y}{t})}{\sum_{z \in Z} \exp(\frac{x^T p_z}{t})}\right), \quad (3)$$

where Z is the set of all proxies, p_y is the target proxy, t is temperature scale. We set $t = 0.05$ following the default setting in [51]. By assigning the label of s_i to s_i^* , we design a chainer loss described as:

$$\mathcal{L}_{cha} = \mathcal{L}_{norm}(\Phi(s_i^*)), \quad (4)$$

with which we can better reduce the domain gap between the sketch and photo domain through the intermediate synthesized images. Besides, we also compute the NormSoftmax loss for the real sketches and photos. The final NormSoftmax loss is computed as:

$$\mathcal{L}_{norm} = \mathcal{L}_{cha} + \mathcal{L}_{norm}(\Phi(s_i)) + \mathcal{L}_{norm}(\Phi(p_j)). \quad (5)$$

Final Objective Function. The final objective function for G , D and Φ is described as:

$$\mathcal{L}(G, D, \Phi) = \mathcal{L}_{adv}(G, D) + \lambda \mathcal{L}_{norm} + \gamma \mathcal{L}_{ide}, \quad (6)$$

where λ and γ are hyper-parameters to balance the contribution of each component. We set $\lambda = 10$ and $\gamma = 0.1$ in our experiments and provide comprehensive experiments using different values of λ and γ in appendix.

Joint Approaching and Centralizing. We optimize G and Φ through a **joint training** manner and the synthesized images are constantly fed into Φ . Through the sketch-to-photo synthesis, we could generate sufficient photo-like examples with high data diversity and force Φ to extract more reliable and effective feature representations under the constraint of \mathcal{L}_{cha} . Besides, by sufficiently generating samples in the latent space, we could promote the generalization ability to unseen categories without requiring access to data from those categories. Our framework is **model-agnostic** and could choose various GAN architectures for synthesis and backbone networks for feature extraction.

Inference. In the test phase, G first generates one photo-like image based on the sketch query and the generated image is used for the retrieval among the photos. We do **not** conduct reverse photo-to-sketch synthesis since we are performing sketch-based image retrieval and the photos are not available in the inference time.

4. Experiments

4.1. Experimental Setup

Datasets. **Sketchy Extended** dataset contains 75,481 sketches and 73,002 photos (12,500 images from [36] and 60,502 images from ImageNet [6] organized by Liu *et al.* [26]) from 125 categories. We follow the same zero-shot data partitioning as [50], in which 21 unseen classes from ImageNet for testing and other classes for training. **TU-Berlin Extended** [10] contains 20,000 sketches evenly distributed over 250 object categories. 204,070 photo images collected by Liu *et al.* [26] are included. The partition

Table 1. The ZS-SBIR performance comparison under various settings on Sketchy Extended dataset: 1) Triplet and NormSoftmax for optimization; and 2) with or without sketch-to-photo synthesis through CycleGAN to mitigate the domain gap.

Loss Type	Synthesis	mAP @200	mAP @all	Prec @100	Prec @200
$\mathcal{L}_{triplet}$	-	35.5	40.8	51.2	47.3
	✓	33.1	38.2	48.1	44.4
\mathcal{L}_{norm}	-	45.2	48.6	60.2	55.7
	✓	43.5	47.5	58.0	53.9

protocol introduced in [37] is used for creating zero-shot training and test sets. 30 randomly picked classes that include at least 400 photo images are used for testing, and other classes are used for training.

Implementation Details. Following the previous methods [7–9, 28, 46, 50, 53], ResNet-50 [19] are adopted as the backbone network. The image resolution and the batch size are 224×224 and 64, respectively. For G , we choose the same architecture of CycleGAN [56]. Please note that we only design the forward sketch-to-photo generator. Furthermore, to reduce the inference time and computational cost, we modify the channel number of the first convolutional layer to 8, and the number of residual blocks to 8, so that our generator is very lightweight. We adopt PatchGAN discriminator [22] architecture for D and also set the channel number of the first convolutional layer to 8 to alleviate the memory burden and computational costs. We provide the detailed neural network configurations in appendix. All the models are warm-up with 1 epoch and have been optimized with 10 epochs. We choose Adam [23] with learning rate $1e^{-3}$ for optimization. Our code is implemented with PyTorch [32] library and the experiments are conducted on the Geforce RTX 3090 GPU.

Evaluation Metrics. Precision ($Prec$) and mean Average Precision (mAP) are two main metrics for the evaluation of ZS-SBIR task [37]. $Prec$ is calculated for top k (i.e., 100, 200) ranked results, and mAP is computed for top k or all ranked results. Higher $Prec$ and mAP indicate better retrieval performance.

4.2. Triplet vs. NormSoftmax

We target to demonstrate that the NormSoftmax loss [51] is more effective than the Triplet loss [14] in the zero-shot setting. We conduct the ZS-SBIR experiments on the Sketchy Extended dataset and the quantitative results are reported in Table 1. To make a fair comparison, all the hyperparameters are set to the same. The Triplet loss can only achieve 35.5% $mAP@200$ while the NormSoftmax loss has achieved 45.2% $mAP@200$, which has gained a large performance improvement. The proxy-based optimization

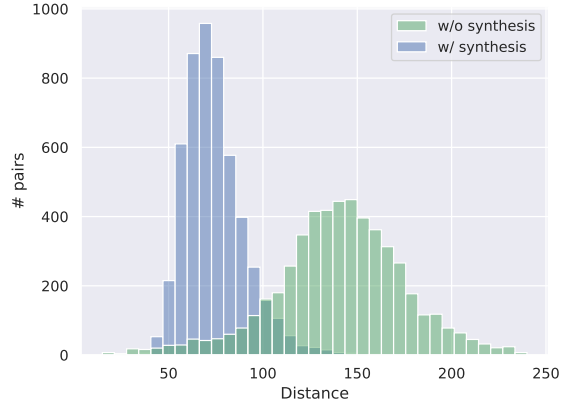


Figure 3. Histograms of sample distances under two settings: 1) between original sketches and real photos (“w/o synthesis”) and 2) between synthesized images and real photos (“w/ synthesis”).

framework could centralize all the samples that belong to the same proxy and prevent the model from only remembering some category-specific samples that have high gradients, which is catastrophic for the generalization ability to unseen categories.

4.3. Two-stage Training vs. Joint Training

In this section, we aim to demonstrate the limitation of the previous two-stage training, which is adopted to mitigate the domain gap between the sketches and photos for the ZS-SBIR. For the first synthesis part, we adopt the vanilla CycleGAN [56] to perform the unpaired image-to-image (I2I) translation between the sketches and photos¹. The train/test split strictly follows the ZS-SBIR setting. After the unpaired I2I model converges, we adopt the trained sketch-to-photo generator for inference and translate all the sketch images into photo-like images. Please note, both training and test sketch images have been translated to the photo domain for further training and testing. We then perform the ZS-SBIR experiments based on the synthesized photo-like images and the real photo images. The original category labels of the sketches are inherited for training. We choose both Triplet loss and the adopted NormSoftmax loss for optimization and the quantitative results are also reported in Table 1. Compared with the counterpart results achieved on the vanilla setting (between the original sketches and photos), there is a slight performance drop regardless of using Triplet loss or NormSoftmax loss.

To dissect this failure, we compute the L_1 distances between 50 randomly sampled instances from each training category under two settings: 1) between the original sketches and the real photos and 2) between the synthe-

¹We adopt the official implementation <https://github.com/junyanz/pytorch-CycleGAN-and-pix2pix> following the default setting.

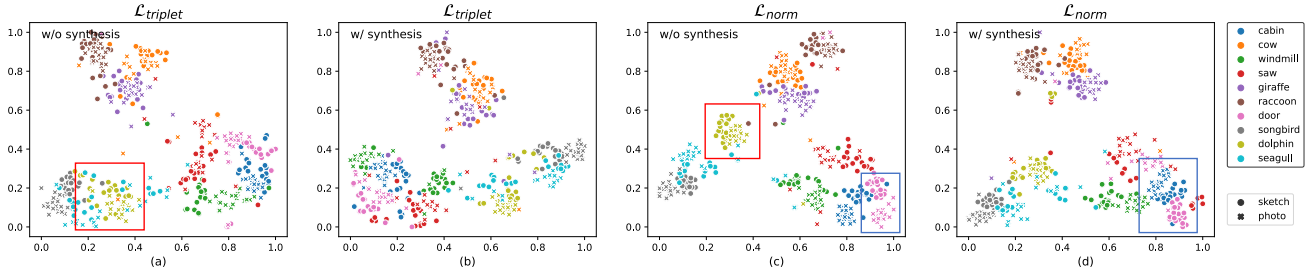


Figure 4. T-SNE visualization of sketch and photo embeddings on Sketchy Extended dataset. We randomly choose 20 samples from 10 unseen test categories for visualization. Different colors refer to different categories. The two-stage training strategy cannot obtain more separable embeddings than the vanilla setting, regardless of using Triplet loss or NormSoftmax loss. We refer the readers to pay more attention on the regions covered by same color boxes for better comparison.

Table 2. Overall comparison of our method and other approaches on Sketchy Extended and TU-Berlin Extended datasets. “†” denotes results obtained by hashing codes, and “-” means that corresponding results are not reported in the original papers. The best and second-best results are bold and underlined, respectively.

Methods	Venue	Semantic	Dim	Sketchy Extended		TU-Berlin Extended	
				mAP@200	Prec@200	mAP@all	Prec@100
DSH [26]	CVPR’17	×	64 [†]	5.9	15.3	12.2	19.8
CVAE [50]	ECCV’18	×	4096	22.5	33.3	0.5	0.1
CSDB [9]	BMVC’19	×	4096	35.8	40.0	25.4	35.5
DSN [48]	IJCAI’21	×	512	-	-	48.1	58.6
NAVE [46]	IJCAI’21	×	512	-	-	49.3	60.7
RPKD [40]	ACM MM’21	×	64 [†]	37.1	48.5	36.1	49.1
			512	<u>50.2</u>	<u>59.8</u>	48.6	61.2
ZSIH [37]	CVPR’18	✓	64 [†]	-	-	22.0	29.1
SEM-PCYC [8]	CVPR’19	✓	64 [†]	-	-	29.3	39.2
			64	47.0	43.7	29.7	42.6
Doodle [7]	CVPR’19	✓	4096	46.1	37.0	10.9	-
SAKE [28]	ICCV’19	✓	64 [†]	35.6	47.7	35.9	48.1
			512	49.7	<u>59.8</u>	47.5	59.9
OCEAN [55]	ICME’20	✓	512	-	-	33.3	46.7
PDFD [49]	IJCAI’20	✓	512	-	-	48.3	60.0
ACNet (Ours)	-	×	64 [†]	48.2	58.1	<u>53.3</u>	<u>63.8</u>
			512	51.7	60.8	57.7	65.8

sized images and the real photos. We provide the distance histogram in Figure 3 to show the domain distance. With the synthesis, the distances have been reduced a lot, which demonstrates that the sketch-to-photo synthesis has indeed effectively mitigated the domain gap. Furthermore, we provide the T-SNE visualization of sketch and photo embeddings on Sketchy Extended dataset in Figure 4 under the four settings of Table 1. The two-stage training strategy cannot obtain more separable embeddings to achieve better ZS-SBIR performance even the synthesis can heavily reduce the domain gap. We attribute this failure to the reason that the gradients of the retrieval module cannot be directly been utilized for the optimization of the synthesis module.

Thus, the synthesis module has no idea how to generate images, which can better serve the image retrieval. We provide a direct comparison between the distribution of the embeddings from the two-stage training and the proposed joint training in Figure 5. As illustrated, our joint training has a strong ability to split the embeddings from different classes, which leads to better ZS-SBIR performance.

4.4. Comparison with SOTA

We compare the proposed method against existing state-of-the-art methods on both Sketchy Extended [50] and TU-Berlin Extended [37] datasets. We also report the experimental results of the methods that introduced the extra se-

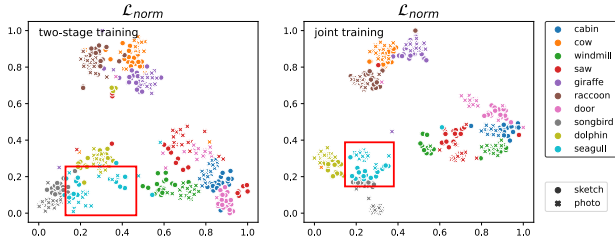


Figure 5. T-SNE visualization of sketch and photo embeddings on Sketchy Extended dataset under the two-stage training and joint training. We refer the readers to pay more attention on the regions covered by same color boxes for better comparison.

Table 3. Ablation studies for the proposed method on TU-Berlin Extended dataset. We adopt the ResNet-50 as our backbone and the embedding dimension is 512. The NormSoftmax loss is used as a baseline.

\mathcal{L}_{norm}	$\mathcal{L}_{adv}\&\mathcal{L}_{cha}$	\mathcal{L}_{ide}	$\mathcal{L}_{norm}(\Phi(s_i))$	mAP @200	mAP @all	Prec @100	Prec @200
✓	-	-	-	47.9	46.5	57.7	55.1
✓	✓	-	-	53.4	54.3	61.9	60.3
✓	✓	✓	-	54.3	54.9	62.9	61.3
✓	✓	-	✓	56.9	56.6	65.2	63.5
✓	✓	✓	✓	57.7	57.7	65.8	64.4

semantic embeddings. The quantitative results of different methods are reported in Table 2. Please note the backbone of the proposed method is ResNet-50. Our method outperforms existing state-of-the-art methods by a large margin even without any specially designed backbones [40] or semantic guidance [55]. Our method has achieved 57.7% $mAP@all$ and 65.8% $Prec@100$ on TU-Berlin Extended dataset [50]. The highest results of other methods are only 49.3% $mAP@all$ and 61.2% $Prec@100$, and our method has achieved 8.4% improvement on $mAP@all$ and 4.6% improvement on $Prec@100$. It is worth noting that our results of using the hashing codes even exceed previous highest performance. We observe that the proposed ACNet has achieved a larger performance gain on the TU-Berlin Extended dataset than the Sketchy Extended dataset. We attribute this phenomenon to the reason that the sketches from TU-Berlin Extended dataset have more abstract sketch representations and fewer fine-grained sketch details. Thus, the proposed ACNet can achieve a large performance gain by making the sketch domain approach to the photo domain. We provide more experimental results of using various embedding dimensions and backbone networks (VGG-16 [38] and ResNet-50 [19]) in appendix.

The qualitative results are shown in Figure 6. We selected three instances from the two datasets to provide an intuitive comparison. The proposed ACNet could effectively find the correct photo given a query sketch. We pro-



Figure 6. Top-5 ZS-SBIR retrieval results from the proposed model (ResNet-50 backbone with 512 embedding dimension) on the Sketchy Extended [50] (first three rows) and TU-Berlin Extended [37] (last three rows) datasets. Correct results are shown with a green border, while incorrect results are shown with a red border.

vide two similar instances from the same category “cow” and the two instances have the same orientation and similar shape representation except for the fine-grained representations on the head part. The proposed method could distinguish these fine-grained representations and provide corresponding desired photos rather than some very similar photos with prominent feature representations, which demonstrates that the proposed ACNet has indeed extracted some common knowledge among the unseen and seen categories. For a more challenging case: the “couch” sketch on the third row of TU-Berlin Extended dataset [37], the fifth retrieved photo belongs to “purse” even though the two categories are conceptually different. We attribute this failure to the reason that the retrieved wrong photo shares very similar structural representations with the real couch photos.

4.5. Ablation Study

Effectiveness of \mathcal{L}_{adv} and \mathcal{L}_{cha} . Considering that \mathcal{L}_{adv} and \mathcal{L}_{cha} are inseparable, we aim to explore the effectiveness of the integration of the two loss functions. On the one hand, the joint training with \mathcal{L}_{cha} could enable the gradients of the retrieval module to back-propagate to the synthesis module, which makes the synthesis better serve the retrieval module. On the other hand, the adversarial loss \mathcal{L}_{adv} could help generate photo-like images with high data diversity and better align the sketch domain and the photo

domain. We have achieved a huge retrieval performance improvement as shown in Table 3 (from 46.5% to 54.3% on $mAP@all$) under the joint training manner with the GAN-based synthesis module.

Effectiveness of \mathcal{L}_{ide} . With the constraint of the pixel-level supervision from reconstructing the photo images, we have marginal improvement than the setting only with the \mathcal{L}_{adv} and \mathcal{L}_{cha} . The $mAP@all$ score increases from 54.3% to 54.9% and the $Prec@100$ score increases by 1% as shown in Table 3.

Effectiveness of $\mathcal{L}_{norm}(\Phi(s_i))$. We have also removed the $\mathcal{L}_{norm}(\Phi(s_i))$ to explore the improvement of this component. Without this, there is a slight retrieval performance drop (from 57.7% to 54.9% on $mAP@all$) according to the quantitative scores reported in Table 3. More experimental analysis can be found in appendix.

4.6. Discussions

Qualitative Sketch-to-photo Synthesis. We provide some visual synthesis results of our sketch-to-photo generator at different epochs in Figure 7. As illustrated, the synthesized images still have visual artifacts, which are not *human-friendly*. We observe the generator has generated obvious boundary (pointed by red arrows) representations, which match the real apple shape better. Thus, we guess that with the constraint of the chainer loss, G aims to synthesize more prominent feature representations, which are more *algorithm-friendly*, recognizable and comparable for Φ . Finally, we also argue that our goal is to promote retrieval performance rather than improve the naturalness and aesthetic quality of the synthesized samples.

Limitations. When given a sketch query that is highly succinct and abstract in Figure 8, it is extremely challenging to judge whether it is “window” or “door” due to the ambiguous correspondences to the photos. Since the sketch-to-photo synthesis module of our method may still fail to generate desired reasonable images with high confidence, our method cannot handle this case well, either.

Broader Impact. Our method has pioneered a new direction to combine synthesis and the downstream visual retrieval task through a joint training manner, in which the gradients of the downstream vision task could be propagated to the synthesis module to tell the generator how to synthesize. Our joint training framework has the potential to be extended to other downstream vision tasks such as semantic segmentation, object detection under some challenging environments (*e.g.*, nighttime, foggy and rainy night), in which the collected visual images have poor visibility. Similarly, we could perform the image synthesis to enhance the image quality to better serve the downstream vision tasks.

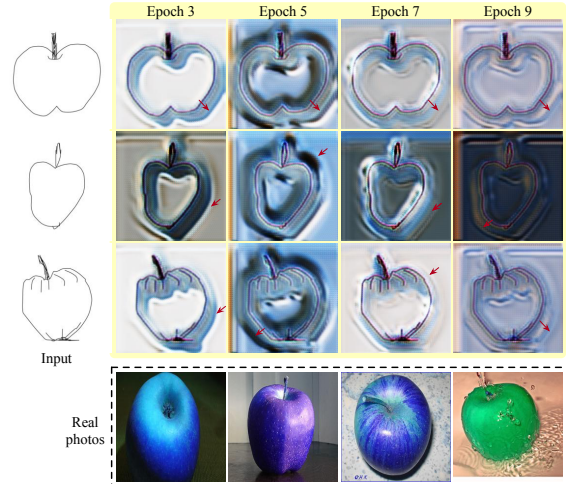


Figure 7. The qualitative sketch-to-photo synthesis results. Images in yellow box indicate the intermediate synthesized images. We also provide some real photos for reference. The sketch-to-photo generator could generate similar shape representations with the real apple photos. Best viewed in color.

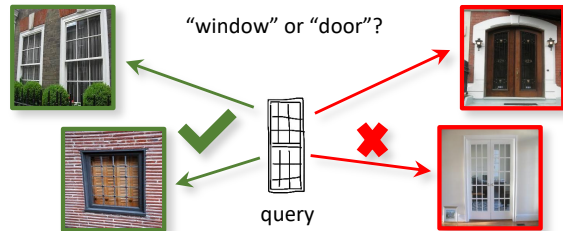


Figure 8. Ambiguous case: the given sketch has the similar structure as “window” and “door”.

5. Conclusion

In this work, we proposed a novel, simple and effective joint synthesis-and-retrieval network called Approaching-and-Centralizing Network (ACNet) for ZS-SBIR and achieved state-of-the-art performance on Sketchy Extended [50] and TU-Berlin Extended [37] datasets. The joint training of the sketch-to-photo synthesis module and the retrieval module could effectively reduce both the domain gap and knowledge gap. The chainer loss is designed to force the retrieval module to extract more reliable and effective feature representations from the synthesized samples even with noise and visual artifacts. The generalization ability to unseen categories can also be enhanced by constantly generating samples with high diversity. Finally, by propagating the gradients of the retrieval module to the synthesis module, we can also tell the generator how to generate samples, which can better serve the downstream vision task. Our joint training framework provides valuable insight on how to integrate the synthesis and other vision tasks.

References

- [1] Pablo Arbeláez, Bharath Hariharan, Chunhui Gu, Saurabh Gupta, Lubomir Bourdev, and Jitendra Malik. Semantic segmentation using regions and parts. In *IEEE Conference on Computer Vision and Pattern Recognition*, pages 3378–3385, 2012. 3
- [2] Ushasi Chaudhuri, Biplab Banerjee, Avik Bhattacharya, and Mihai Datcu. CrossATNet—a novel cross-attention based framework for sketch-based image retrieval. *Image and Vision Computing*, 104:104003, 2020. 1, 2
- [3] Tao Chen, Ming-Ming Cheng, Ping Tan, Ariel Shamir, and Shi-Min Hu. Sketch2photo: Internet image montage. *ACM Transactions on Graphics*, 28(5):1–10, 2009. 2, 3
- [4] Wengling Chen and James Hays. SketchyGAN: Towards diverse and realistic sketch to image synthesis. In *IEEE Conference on Computer Vision and Pattern Recognition*, pages 9416–9425, 2018. 3
- [5] Cheng Deng, Xinxun Xu, Hao Wang, Muli Yang, and Dacheng Tao. Progressive cross-modal semantic network for zero-shot sketch-based image retrieval. *IEEE Transactions on Image Processing*, 29:8892–8902, 2020. 2
- [6] Jia Deng, Wei Dong, Richard Socher, Li-Jia Li, Kai Li, and Li Fei-Fei. ImageNet: A large-scale hierarchical image database. In *IEEE Conference on Computer Vision and Pattern Recognition*, pages 248–255, 2009. 4
- [7] Sounak Dey, Pau Riba, Anjan Dutta, Josep Lladós, and Yi-Zhe Song. Doodle to search: Practical zero-shot sketch-based image retrieval. In *IEEE Conference on Computer Vision and Pattern Recognition*, pages 2179–2188, 2019. 2, 5, 6
- [8] Anjan Dutta and Zeynep Akata. Semantically tied paired cycle consistency for zero-shot sketch-based image retrieval. In *IEEE Conference on Computer Vision and Pattern Recognition*, pages 5089–5098, 2019. 2, 5, 6
- [9] Titir Dutta and Soma Biswas. Style-guided zero-shot sketch-based image retrieval. In *British Machine Vision Conference*, page 9, 2019. 2, 5, 6
- [10] Mathias Eitz, James Hays, and Marc Alexa. How do humans sketch objects? *ACM Transactions on Graphics*, 31(4):1–10, 2012. 4
- [11] Mathias Eitz, Kristian Hildebrand, Tamy Boubekeur, and Marc Alexa. Sketch-based image retrieval: Benchmark and bag-of-features descriptors. *IEEE Transactions on Visualization and Computer Graphics*, 17:1624–1636, 2010. 1, 2
- [12] Mathias Eitz, Ronald Richter, Kristian Hildebrand, Tamy Boubekeur, and Marc Alexa. Photosketcher: Interactive sketch-based image synthesis. *IEEE Computer Graphics and Applications*, 31:56–66, 2011. 3
- [13] Anibal Fuentes and Jose M Saavedra. Sketch-QNet: A Quadruplet ConvNet for color sketch-based image retrieval. In *IEEE Conference on Computer Vision and Pattern Recognition*, pages 2134–2141, 2021. 2
- [14] Weifeng Ge. Deep metric learning with hierarchical triplet loss. In *European Conference on Computer Vision*, pages 269–285, 2018. 2, 5, 12
- [15] Arnab Ghosh, Richard Zhang, Puneet K Dokania, Oliver Wang, Alexei A Efros, Philip HS Torr, and Eli Shechtman. Interactive sketch & fill: Multiclass sketch-to-image translation. In *International Conference on Computer Vision*, pages 1171–1180, 2019. 3
- [16] Yoav Goldberg and Omer Levy. Word2vec explained: Deriving mikolov et al.’s negative-sampling word-embedding method. *arXiv preprint arXiv:1402.3722*, 2014. 3
- [17] Nuno Gracias, Mohammad Mahoor, Shahriar Negahdaripour, and Arthur Gleason. Fast image blending using watersheds and graph cuts. *Image and Vision Computing*, 27(5):597–607, 2009. 3
- [18] Raia Hadsell, Sumit Chopra, and Yann LeCun. Dimensionality reduction by learning an invariant mapping. In *IEEE Conference on Computer Vision and Pattern Recognition*, pages 1735–1742, 2006. 2
- [19] Kaiming He, Xiangyu Zhang, Shaoqing Ren, and Jian Sun. Deep residual learning for image recognition. In *IEEE Conference on Computer Vision and Pattern Recognition*, pages 770–778, 2016. 4, 5, 7, 12
- [20] Alexander Hermans, Lucas Beyer, and Bastian Leibe. In defense of the triplet loss for person re-identification. *arXiv preprint arXiv:1703.07737*, 2017. 2
- [21] Rui Hu and John Collomosse. A performance evaluation of gradient field hog descriptor for sketch based image retrieval. *Computer Vision and Image Understanding*, 117:790–806, 2013. 1, 2
- [22] Phillip Isola, Jun-Yan Zhu, Tinghui Zhou, and Alexei A Efros. Image-to-image translation with conditional adversarial networks. In *IEEE Conference on Computer Vision and Pattern Recognition*, pages 1125–1134, 2017. 5
- [23] Diederik P Kingma and Jimmy Ba. Adam: A method for stochastic optimization. In *International Conference on Learning Representations*, 2015. 5
- [24] Jiangtong Li, Zhixin Ling, Li Niu, and Liqing Zhang. Zero-shot sketch-based image retrieval with structure-aware asymmetric disentanglement. *arXiv preprint arXiv:1911.13251*, 2019. 1, 2
- [25] Zeyu Li, Cheng Deng, Kun Wei, Wei Liu, and Dacheng Tao. Learning semantic priors for texture-realistic sketch-to-image synthesis. *Neurocomputing*, 464:130–140, 2021. 3
- [26] Li Liu, Fumin Shen, Yuming Shen, Xianglong Liu, and Ling Shao. Deep sketch hashing: Fast free-hand sketch-based image retrieval. In *IEEE Conference on Computer Vision and Pattern Recognition*, pages 2862–2871, 2017. 1, 2, 3, 4, 6
- [27] Ming-Yu Liu, Thomas Breuel, and Jan Kautz. Unsupervised image-to-image translation networks. In *Annual Conference on Neural Information Processing Systems*, pages 700–708, 2017. 3
- [28] Qing Liu, Lingxi Xie, Huiyu Wang, and Alan L Yuille. Semantic-aware knowledge preservation for zero-shot sketch-based image retrieval. In *International Conference on Computer Vision*, pages 3662–3671, 2019. 2, 5, 6
- [29] Runtao Liu, Qian Yu, and Stella X Yu. Unsupervised sketch to photo synthesis. In *European Conference on Computer Vision*, pages 36–52, 2020. 2, 3
- [30] Peng Lu, Gao Huang, Hangyu Lin, Wenming Yang, Guodong Guo, and Yanwei Fu. Domain-aware SE net-

- work for sketch-based image retrieval with multiplicative euclidean margin softmax. In *ACM International Conference on Multimedia*, pages 3418–3426, 2021. [2](#)
- [31] Yair Movshovitz-Attias, Alexander Toshev, Thomas K Leung, Sergey Ioffe, and Saurabh Singh. No fuss distance metric learning using proxies. In *International Conference on Computer Vision*, pages 360–368, 2017. [2](#)
- [32] Adam Paszke, Sam Gross, Francisco Massa, Adam Lerer, James Bradbury, Gregory Chanan, Trevor Killeen, Zeming Lin, Natalia Gimelshein, Luca Antiga, et al. PyTorch: An imperative style, high-performance deep learning library. In *Annual Conference on Neural Information Processing Systems*, pages 8026–8037, 2019. [5](#)
- [33] Jeffrey Pennington, Richard Socher, and Christopher D Manning. Glove: Global vectors for word representation. In *Conference on Empirical Methods in Natural Language Processing*, pages 1532–1543, 2014. [3](#)
- [34] Leo Sampaio Ferraz Ribeiro, Tu Bui, John Collomosse, and Moacir Ponti. Sketchformer: Transformer-based representation for sketched structure. In *IEEE Conference on Computer Vision and Pattern Recognition*, pages 14153–14162, 2020. [3](#)
- [35] Aneeshan Sain, Ayan Kumar Bhunia, Yongxin Yang, Tao Xiang, and Yi-Zhe Song. StylemeUp: Towards style-agnostic sketch-based image retrieval. In *IEEE Conference on Computer Vision and Pattern Recognition*, pages 8504–8513, 2021. [2](#)
- [36] Patsorn Sangkloy, Nathan Burnell, Cusuh Ham, and James Hays. The sketchy database: Learning to retrieve badly drawn bunnies. *ACM Transactions on Graphics*, 35(4):1–12, 2016. [4](#)
- [37] Yuming Shen, Li Liu, Fumin Shen, and Ling Shao. Zero-shot sketch-image hashing. In *IEEE Conference on Computer Vision and Pattern Recognition*, pages 3598–3607, 2018. [2, 5, 6, 7, 8, 11, 15](#)
- [38] Karen Simonyan and Andrew Zisserman. Very deep convolutional networks for large-scale image recognition. In *International Conference on Learning Representations*, 2015. [7, 12](#)
- [39] Eu Wern Teh, Terrance DeVries, and Graham W Taylor. ProxyNCA++: Revisiting and revitalizing proxy neighborhood component analysis. In *European Conference on Computer Vision*, pages 448–464, 2020. [2](#)
- [40] Jialin Tian, Xing Xu, Zheng Wang, Fumin Shen, and Xin Liu. Relationship-preserving knowledge distillation for zero-shot sketch based image retrieval. In *ACM International Conference on Multimedia*, page 5473–5481, 2021. [6, 7](#)
- [41] Pablo Torres and Jose M Saavedra. Compact and effective representations for sketch-based image retrieval. In *IEEE Conference on Computer Vision and Pattern Recognition*, pages 2115–2123, 2021. [2](#)
- [42] Osman Tursun, Simon Denman, Sridha Sridharan, Ethan Goan, and Clinton Fookes. An efficient framework for zero-shot sketch-based image retrieval. *arXiv preprint arXiv:2102.04016*, 2021. [2](#)
- [43] Luo Wang, Xueming Qian, Xingjun Zhang, and Xingsong Hou. Sketch-based image retrieval with multi-clustering ranking. *IEEE Transactions on Circuits and Systems for Video Technology*, 30:4929–4943, 2019. [1, 2](#)
- [44] Luo Wang, Xueming Qian, Yuting Zhang, Jialie Shen, and Xiaochun Cao. Enhancing sketch-based image retrieval by CNN semantic re-ranking. *IEEE Transactions on Cybernetics*, 50:3330–3342, 2019. [1, 2](#)
- [45] Sheng-Yu Wang, David Bau, and Jun-Yan Zhu. Sketch your own GAN. In *International Conference on Computer Vision*, pages 14050–14060, 2021. [3](#)
- [46] Wenjie Wang, Yufeng Shi, Shiming Chen, Qinmu Peng, Feng Zheng, and Xinge You. Norm-guided adaptive visual embedding for zero-shot sketch-based image retrieval. In *International Joint Conference on Artificial Intelligence*, pages 1106–1112, 2021. [2, 3, 5, 6](#)
- [47] Xun Wang, Xintong Han, Weilin Huang, Dengke Dong, and Matthew R Scott. Multi-similarity loss with general pair weighting for deep metric learning. In *IEEE Conference on Computer Vision and Pattern Recognition*, pages 5022–5030, 2019. [2](#)
- [48] Zhipeng Wang, Hao Wang, Jiexi Yan, Aming Wu, and Cheng Deng. Domain-smoothing network for zero-shot sketch-based image retrieval. In *International Joint Conference on Artificial Intelligence*, pages 1143–1149, 2021. [6](#)
- [49] Xinxun Xu, Muli Yang, Yanhua Yang, and Hao Wang. Progressive domain-independent feature decomposition network for zero-shot sketch-based image retrieval. In *International Joint Conference on Artificial Intelligence*, pages 984–990, 2021. [2, 6](#)
- [50] Sasi Kiran Yelamarthi, Shiva Krishna Reddy, Ashish Mishra, and Anurag Mittal. A zero-shot framework for sketch based image retrieval. In *European Conference on Computer Vision*, pages 300–317, 2018. [1, 2, 4, 5, 6, 7, 8, 11, 14](#)
- [51] Andrew Zhai and Hao-Yu Wu. Classification is a strong baseline for deep metric learning. In *British Machine Vision Conference*, page 91, 2019. [2, 4, 5, 12](#)
- [52] Jingyi Zhang, Fumin Shen, Li Liu, Fan Zhu, Mengyang Yu, Ling Shao, Heng Tao Shen, and Luc Van Gool. Generative domain-migration hashing for sketch-to-image retrieval. In *European Conference on Computer Vision*, pages 297–314, 2018. [3](#)
- [53] Zhaolong Zhang, Yuejie Zhang, Rui Feng, Tao Zhang, and Weiguo Fan. Zero-shot sketch-based image retrieval via graph convolution network. In *AAAI Conference on Artificial Intelligence*, pages 12943–12950, 2020. [2, 5](#)
- [54] Ziqiang Zheng, Yang Wu, Xinran Han, and Jianbo Shi. ForkGAN: Seeing into the rainy night. In *European Conference on Computer Vision*, pages 155–170, 2020. [3](#)
- [55] Jiawen Zhu, Xing Xu, Fumin Shen, Roy Ka-Wei Lee, Zheng Wang, and Heng Tao Shen. OCEAN: A dual learning approach for generalized zero-shot sketch-based image retrieval. In *IEEE International Conference on Multimedia & Expo*, pages 1–6, 2020. [2, 6, 7](#)
- [56] Jun-Yan Zhu, Taesung Park, Phillip Isola, and Alexei A Efros. Unpaired image-to-image translation using cycle-consistent adversarial networks. In *International Conference on Computer Vision*, pages 2223–2232, 2017. [3, 5, 11](#)

Appendix

In this appendix, we first provide the implementation details of our sketch-to-photo generator and corresponding discriminator. Then we provide more experimental results to demonstrate that the NormSoftmax is better than Triplet and the proposed joint training scheme is more effective than two-stage training scheme for the ZS-SBIR task. The results of using various backbones and embedding sizes are also included. More qualitative results are provided to give an intuitive comparison. Finally, we provide further ablation studies to explore the sensitiveness and effectiveness of the proposed ACNet to different hyper parameters.

A. Implementation Details

We follow the generator architecture of the vanilla CycleGAN [56] and design our sketch-to-photo generator.

Generator architecture. For G , we first adopt the Conv-InstanceNorm-ReLU (**CIR** for short) block with kernel size 7 and stride size 1 for the sketches. Then two CIR blocks with kernel size 3 and stride size 2 to achieve down-sampling are conducted. To enlarge the information capacity, G combines 8 residual blocks (**RB**) to stack residual information. For the residual blocks, the kernel size is 3 and the stride size is 1. As for the reverse up-sampling stage, another 3 Deconv-InstanceNorm-ReLU (**DIR**) blocks are adopted. Finally, a Tanh activation is adopted to obtain the normalized photo-like images.

Discriminator architecture. We first apply one Conv-LeakyReLU layer (**CLR**) with kernel size 4 and stride size 2 to achieve down-sampling. Then three Conv-InstanceNorm-LeakyReLU layers (**CILR**) with kernel size 4 are adopted. The slope for the LeakyReLU is 0.2. We finally obtain the logit output to perform the real/fake discrimination after one convolution layer with kernel size 4.

We refer the readers to check Table 4 and Table 5 for more details. We also provide the corresponding ZS-SBIR experiments of using different architectures of G in Section C.2.

B. More Experiments

B.1. Triplet vs. NormSoftmax

Following the same experimental setting on the Sketchy Extended [50] dataset as presented in the main text, we chose the vanilla Triplet loss and NormSoftmax loss and perform the ZS-SBIR experiments on the TU-Berlin Extended [37] dataset. The quantitative results are reported in Table 6. We can observe that the NormSoftmax outperforms the Triplet by a large margin (47.9% vs. 38.1% on $mAP@200$ score), which indicates that the proxy-based loss has a significant priority over the triplets-based loss on ZS-SBIR task.

Table 4. The network architecture of G . c is the number of channels of the first convolution layer.

G (sketch-to-photo generator)				
Module Type	Kernel Size	Stride Size	Channel Number	Padding Type
CIR	7	1	$c = 8$	reflect
	3	2	$16 (2 \times c)$	zero
	3	2	$32 (4 \times c)$	zero
RB	3	1	$32 (4 \times c)$	reflect
	3	1	$32 (4 \times c)$	reflect
	3	1	$32 (4 \times c)$	reflect
	3	1	$32 (4 \times c)$	reflect
	3	1	$32 (4 \times c)$	reflect
	3	1	$32 (4 \times c)$	reflect
	3	1	$32 (4 \times c)$	reflect
	3	1	$32 (4 \times c)$	reflect
DIR	3	2	$16 (2 \times c)$	zero
	3	2	8	zero
	7	1	3	reflect
Tanh	-	-	3	reflect

Table 5. The network architecture of D . c is the number of channels of the first convolution layer.

D (Discriminator)			
Module Type	Kernel Size	Stride Size	Channel Number
CLR	4	2	$c = 8$
CILR	4	2	$16 (2 \times c)$
	4	2	$32 (4 \times c)$
	4	1	$64 (8 \times c)$
Conv	4	1	1

B.2. Two-stage Training vs. Joint Training

For the two-stage training strategy, we first adopt the vanilla CycleGAN [56] to perform the unpaired image-to-image (I2I) translation between the sketches and photos on the TU-Berlin Extended dataset. After the unpaired I2I model converges, we adopt the trained sketch-to-photo generator for inference and translate all the sketches into photo-like images. Please note, both training and test sketches have been translated to the photo domain for further training and testing. We then perform the ZS-SBIR experiments based on the synthesized photo-like images and the real photos. The original category labels of the sketches are inherited for training. We choose both Triplet loss and the adopted NormSoftmax loss for optimization and the quantitative results are also reported in Table 6.

We can obtain better results based on \mathcal{L}_{norm} by ap-

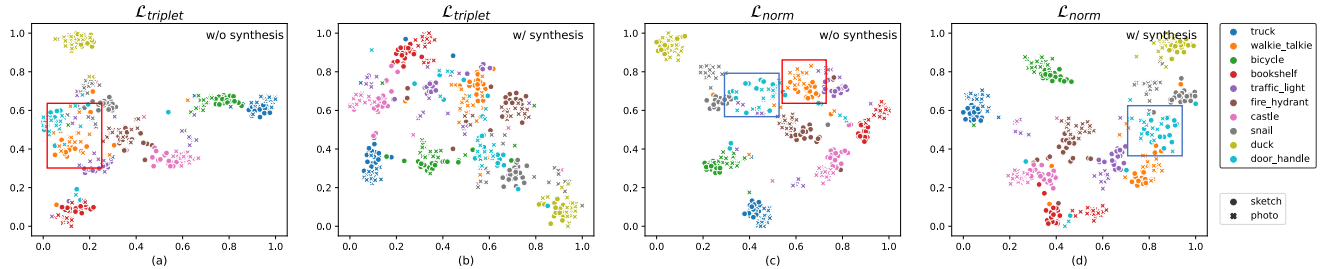


Figure 9. T-SNE visualization of sketch and photo embeddings on TU-Berlin Extended dataset. We randomly choose 20 samples from 10 unseen test categories for visualization. Different colors refer to different categories. The two-stage training strategy cannot obtain more separable embeddings than the vanilla setting, regardless of using Triplet loss or NormSoftmax loss. We refer the readers to pay more attention to the regions covered by the same color boxes for better comparison.

Table 6. The ZS-SBIR performance comparison under various settings on TU-Berlin Extended dataset: 1) Triplet and NormSoftmax for optimization; and 2) with or without sketch-to-photo synthesis through CycleGAN to mitigate the domain gap.

Loss Type	Synthetic	mAP @200	mAP @all	Prec @100	Prec @200
$\mathcal{L}_{triplet}$	-	38.1	36.8	49.8	47.1
	✓	36.3	35.2	47.7	45.4
\mathcal{L}_{norm}	-	47.9	46.5	57.7	55.1
	✓	48.4	46.6	58.0	55.6

proaching the sketch domain to the photo domain. We attribute this improvement to the reason that the sketch-to-photo synthesis module could help the retrieval module capture more effective feature representations. In contrast, there is a performance drop while using the Triplet loss for optimization, which also indicates that the NormSoftmax [51] has a stronger ability to coordinate the real samples and the synthesized samples than Triplet [14]. The NormSoftmax is more compatible with the sketch-to-photo synthesis for data transformation to mitigate the domain gap.

We further compute the L_1 distances between 50 randomly sampled instances from each training category under two settings: 1) between the original sketches and the real photos and 2) between the synthesized images and the real photos. We provide the distance histogram in Figure 10 to show the domain distance. Since the sketches from the TU-Berlin Extended dataset are highly abstract, succinct and exaggerated, with the synthesis, we can reduce the domain gap to some extent.

Furthermore, we provide the T-SNE visualization of sketch and photo embeddings on TU-Berlin Extended dataset in Figure 9 under the four settings of Table 6. The two-stage training strategy cannot obtain much more separable embeddings to achieve a large ZS-SBIR performance

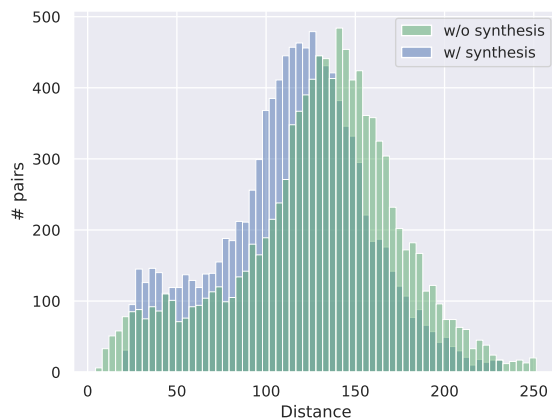


Figure 10. Histograms of sample distances under two settings: 1) between original sketches and real photos (“w/o synthesis”) and 2) between synthesized images and real photos (“w/ synthesis”). The experiments are conducted on the TU-Berlin Extended dataset. Since the sketches of this dataset are highly abstract, succinct and exaggerated, the vanilla CycleGAN could only mitigate the domain gap to some extent.

gain. We attribute this failure to the reason that the gradients of the retrieval module cannot be directly been utilized for the optimization of the synthesis module. Thus, the synthesis module has no idea how to generate images, which can better serve the image retrieval. We provide a direct comparison between the distribution of the embeddings from the two-stage training and the proposed joint training in Figure 11. As illustrated, our joint training has a strong ability to split the embeddings from different classes, which leads to better ZS-SBIR performance.

B.3. Various Backbones and Embedding Sizes

In this section, we aim to explore the effectiveness and sensitiveness of choosing various backbone networks: ResNet-50 [19] and VGG-16 [38]. We conduct the ZS-SBIR experiments on both the Sketchy Extended and TU-

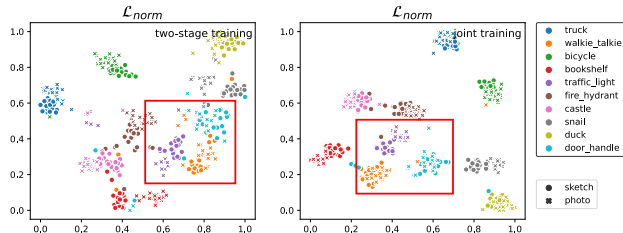


Figure 11. T-SNE visualization of sketch and photo embeddings on TU-Berlin Extended dataset under the two-stage training and joint training. We refer the readers to pay more attention on the regions covered by same color boxes for better comparison.

Table 7. Overall comparison of our method with different backbone networks and embedding sizes on Sketchy Extended and TU-Berlin Extended datasets. The best scores are bolded.

Backbone	Dim	Sketchy Extended		TU-Berlin Extended	
		mAP @200	Prec @200	mAP @all	Prec @100
VGG-16	64	32.6	44.7	37.1	50.6
	512	38.3	49.3	43.9	58.1
	4096	40.0	50.8	47.9	62.3
ResNet-50	64	43.0	52.7	44.9	57.2
	512	51.7	60.8	57.7	65.8
	4096	51.1	60.0	58.6	64.6

Berlin Extended datasets. All the quantitative results under various settings are reported in Table 7. With the same embedding size, we can obtain better results based on the ResNet-50 than the VGG-16. The proposed ACNet could achieve a very impressive 58.6% $mAP@all$ score on the TU-Berlin Extended dataset by choosing the ResNet-50 with 4096 embedding size as the backbone network.

B.4. More Qualitative Results

We provide more visual retrieval results on the Sketchy Extended and TU-Berlin Extended datasets in Figure 12 and Figure 13, respectively. We selected eight instances from the two datasets to provide an intuitive comparison. The proposed ACNet could effectively find the correct photo given a query sketch.

C. Ablation Studies

C.1. Component Dissection

We have also performed the ablation studies on the Sketchy Extended dataset to show the effectiveness of each component of the proposed ACNet. All the quantitative results are reported in Table 8. With only the NormSoftmax loss, the proposed method could only achieve a 45.2% $mAP@200$ score. By combining the sketch-to-photo syn-

Table 8. Ablation studies for the proposed method on Sketchy Extended dataset. We adopt the ResNet-50 as our backbone and the embedding dimension is 512. The NormSoftmax loss is used as a vanilla baseline.

\mathcal{L}_{norm}	$\mathcal{L}_{adv}&\mathcal{L}_{cha}$	\mathcal{L}_{ide}	$\mathcal{L}_{norm}(\Phi(s_i))$	mAP @200	mAP @all	Prec @100	Prec @200
✓	-	-	-	45.2	48.6	60.2	55.7
✓	✓	-	-	47.8	52.7	60.9	57.1
✓	✓	✓	-	48.4	53.0	61.4	57.6
✓	✓	-	✓	49.7	53.7	62.2	58.7
✓	✓	✓	✓	51.7	55.9	64.3	60.8

Table 9. Overall comparison of our method with different number of channels on Sketchy Extended and TU-Berlin Extended datasets. The best and second-best results are bold and underlined, respectively.

Number of Channels (c)	Sketchy Extended		TU-Berlin Extended	
	mAP @200	Prec @200	mAP @all	Prec @100
4	51.9	60.9	56.8	65.5
8	51.7	<u>60.8</u>	57.7	<u>65.8</u>
16	<u>51.8</u>	60.5	<u>56.9</u>	66.1
32	50.9	60.1	56.3	65.1
64	49.0	58.5	54.1	62.6

thesis in a joint training manner, we can increase the $mAP@200$ score from 45.2% to 47.8%. The identity loss could also help promote the synthesis quality and thus lead to a performance gain (from 47.8% to 48.4% on $mAP@200$ score). Finally, with the constraint of $\mathcal{L}_{norm}(\Phi(s_i))$, the proposed method could better mitigate the domain gap between the sketches and the photos.

C.2. GAN Capacity

We also explore the influences of choosing different architectures for G and D on the final ZS-SBIR results. We conduct the corresponding experiments in two ways. We first set the number of channels c to different values for both G and D . The quantitative results are reported in Table 9. We observe that we can achieve better results when using a lightweight architecture for G and D . We guess that it is more possible for the model with a bigger network capacity to introduce the noise and uncertainty for the downstream retrieval module.

Later, we design different architectures for G by choosing different numbers of residual blocks and the results are reported in Table 10. An appropriate number (*e.g.*, 6 or 8) of residual block could achieve the best ZS-SBIR results.



Figure 12. Top-10 ZS-SBIR retrieval results from the proposed model (ResNet-50 backbone with 512 embedding dimension) on the Sketchy Extended [50] dataset. Correct results are shown with a green border, while incorrect results are shown with a red border.

Table 10. Overall comparison of our method with different number of blocks on Sketchy Extended and TU-Berlin Extended datasets. The best and second-best results are bold and underlined, respectively.

Number of Blocks	Sketchy Extended		TU-Berlin Extended	
	mAP @200	Prec @200	mAP @all	Prec @100
4	<u>50.5</u>	<u>59.8</u>	55.9	<u>65.1</u>
6	50.1	59.2	57.8	65.8
8	51.7	60.8	<u>57.7</u>	65.8
9	49.6	59.1	55.4	64.6

C.3. Selection of λ and γ

Rethink our final objective function:

$$\mathcal{L}(G, D, \Phi) = \mathcal{L}_{adv}(G, D) + \lambda \mathcal{L}_{norm} + \gamma \mathcal{L}_{ide}, \quad (7)$$

Table 11. Overall comparison of our method with different hyper parameters on Sketchy Extended dataset and TU-Berlin Extended dataset.

λ	γ	Sketchy Extended		TU-Berlin Extended	
		mAP @200	Prec @200	mAP @all	Prec @100
0.1	10	46.9	56.7	54.9	63.7
1.0	1.0	49.9	59.2	56.5	65.2
10	0.1	51.7	60.8	57.7	65.8

there are two hyper parameters to balance the contribution of each loss function. To explore the sensitiveness of the proposed ACNet to the two hyper parameters, we have designed three experiments of using different combinations of λ and γ : ($\lambda = 0.1, \gamma = 10$), ($\lambda = 1.0, \gamma = 1.0$) and ($\lambda = 10, \gamma = 0.1$). The quantitative comparison is reported in Table 11. As observed, the proposed ACNet could

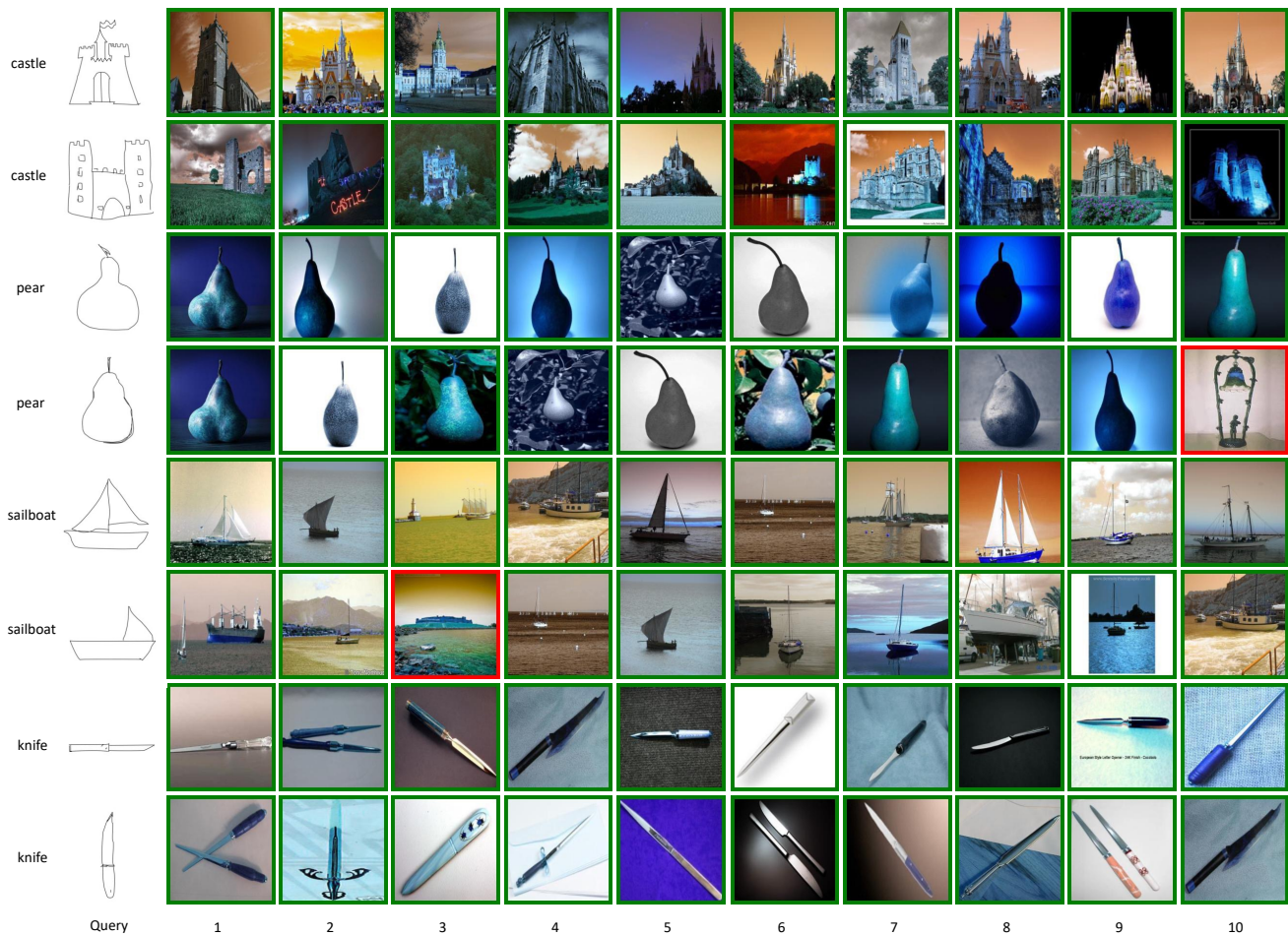


Figure 13. Top-10 ZS-SBIR retrieval results from the proposed model (ResNet-50 backbone with 512 embedding dimension) on the TU-Berlin Extended [37] dataset. Correct results are shown with a green border, while incorrect results are shown with a red border.

achieve the highest scores when $\lambda = 10$ and $\gamma = 0.1$.